PAPER

Check for updates

Preparation of S–N co-doped CoFe$_2$O$_4$@rGO@TiO$_2$ nanoparticles and their superior UV-Vis light photocatalytic activities

Fengyu Wei, [iD] * Hui Wang, Wei Ran, Tao Liu and Xueting Liu

A S–N co-doped CoFe$_2$O$_4$@rGO@TiO$_2$ (CFGT-S/N) nanocomposite was successfully synthesized *via* a facile vapor-thermal method. XRD, XPS, FT-IR and FETEM results confirmed that N and S were co-doped into the lattice of TiO$_2$. Photocatalytic tests indicated that CFGT-S/N exhibited excellent UV-Vis photocatalytic activity for decompositions of different organic dyes, including methyl orange (MO), rhodamine B (RhB) and methylene blue (MB). Particularly, the photocatalytic degradation rate of MO was about 33% higher than that when using P25 under visible light irradiation. The higher UV-Vis light photocatalytic activity of CFGT-S/N can be attributed to the synergetic effects of the strong absorption of visible light, the narrow band gap, improved separation of photo-generated electron/hole pairs, and the enhancement of the enrichment of pollutant dye molecules by S, N co-doping, CoFe$_2$O$_4$ and rGO. Moreover, this photocatalyst was superparamagnetic, which enables it to be easily recovered by an external magnetic field, and maintained stable photocatalytic efficiency over five cycles. Hence, CFGT-S/N with its highly efficient, recoverable and stable photocatalytic properties shows great potential for environmental treatment.

1 Introduction

Titanium dioxide (TiO$_2$) is a conventional photocatalyst widely used for the degradation of organic pollutants in wastewater, because of its powerful oxidizing power, high benefit-to-cost ratio, nontoxicity, and its extended stability against photo- and chemical corrosion.[1] However, TiO$_2$ can be activated only under UV-light irradiation due to its wide bandgap (E$_g$ = 3.2 eV for anatase TiO$_2$), which might hinder its practical application.[2] To improve the utilization of solar light, a lot of researchers have shown that doping TiO$_2$ with non-metal elements such as C, N, F, S and B could be an effective strategy.[3–7] In order to further achieve photocatalytic activity, co-doping TiO$_2$ with two or three non-metal elements has attracted much attention, such as N–F,[5,8] N–B,[9] C–N,[10] S–N,[11,12] S, N and C,[3,13] and so on. Density functional theory (DFT) calculations have shown that the doping S, N elements could lower the band gap of TiO$_2$ effectively.[14] Our previous work[12] also proved that a S–N co-doped anatase nanosized TiO$_2$ photocatalyst exhibited a high activity for the decomposition of methyl orange under both UV-light and Vis-light irradiation comparing to S-doped TiO$_2$ and undoped TiO$_2$ due to the synergetic effects induced by N and S co-doping.

Anhui Province Key Laboratory of Advanced Catalytic Materials and Reaction Engineering, School of Chemistry and Chemical Engineering, Hefei University of Technology, Hefei 230009, P. R. China. E-mail: weifyliuj@hfut.edu.cn; Fax: +86 551 62901548; Tel: +86 551 62901548

In recent years, graphene has attracted much attention because it is an ideal electron acceptor for nanocomposites during the photocatalytic process, which can slow the recombination of photoexcited electron–hole pairs, increasing the charge transfer rate of electrons.[15,16] What is more, the high surface area of graphene based on nanocomposites can provide more active sites to adsorb reactant molecules. Many researchers have indicated that graphene–TiO$_2$ hybrid materials exhibited enhanced photoactivity over bare TiO$_2$ during decomposition of organic dyes in water.[17–19]

Although the photocatalytic performance of graphene–TiO$_2$ nanocomposites has improved, separation and recycling is still a major bottleneck for their application. To solve the separation of the catalyst, a method to integrate graphene–TiO$_2$ with magnetic nanocomposites, such as Fe$_3$O$_4$,[17,20] CoFe$_2$O$_4$,[21] ZnFe$_2$O$_4$,[22] and so on, was proposed, which enables recycling and removal of the magnetic particles by an external magnetic field. Wherein, cobalt ferrite (CoFe$_2$O$_4$) with a spinel crystallographic structure and a narrow band-gap exhibited a superior magnetic behavior and visible light response.[21,23–25] But these TiO$_2$ and magnetic nanoparticles loaded on the surface of graphene sheets may have the defects of detachment and could not effectively prevent photodissolution and recombination of electron–hole pairs, which decreases their photocatalytic activity.[26,27] Recently, Yang et al.[28] synthesized a ternary nanocomposite with TiO$_2$ nanoparticles anchored on reduced graphene oxide (rGO)-encapsulated Fe$_3$O$_4$ spheres (Fe$_3$O$_4$@rGO@TiO$_2$) by an electrostatic layer-by-layer method.

The results showed that the three components of $Fe_3O_4@$-rGO@TiO_2 possessed synergistic effect, and the catalyst exhibited enhancing catalytic activity for the degradation of MB. However, its preparation was more complicated, and visible light activity was high only in the presence of H_2O_2.

Recently, our group has prepared a magnetic $CoFe_2O_4@$-rGO core–shell nanocomposite as an efficient adsorbent for removal of organic pollutants, which had excellent adsorption properties and selectivity.[29] On this basis, we provided a facile and feasible way to synthesize S and N co-doped $CoFe_2O_4@$-rGO@TiO_2 composites, which possessed excellent photocatalytic activity under both ultraviolet and visible light irradiation. Physical and chemical characterizations of catalysts were conducted, and the photocatalytic activity was evaluated in the photocatalytic degradation of organic dyes. This work may be helpful for preparing novel UV-light and Vis-light photocatalysts with good performance and recoverable ability.

2 Experimental

2.1 Materials and chemicals

Graphite powder, ethylene glycol (EG), polyethylene 2000 (PEG 2000), anhydrous ferric chloride ($FeCl_3$), cobalt(II) chloride hexahydrate ($CoCl_2 \cdot 6H_2O$), sodium acetate (NaAc), tetrabutyltitanate (TBOT), thiourea, methylene blue, methylene orange, rhodamine B and other reagents were purchased from Sinopharm Group Chemical Reagent Co (China). All chemicals used were analytical grade and were used without further purification.

2.2 Preparation of the S, N co-doped $CoFe_2O_4@$rGO@TiO_2 nanocomposite

Graphene oxide was prepared by a modified Hummers method.[30] The preparation of the binary core–shell composites $CoFe_2O_4@$rGO (CFG) using a one-step hydrothermal method has been reported by our laboratory.[29] The S–N co-doped $CoFe_2O_4@$rGO@TiO_2 nanocomposite was synthesized *via* the vapor-thermal method[20] with minor modifications. Briefly, 0.8 mL of TBOT and 60 mg of thiourea were added into 10 mL ethanol, and then the beaker was placed in an ultrasonic bath to completely dissolve the resulting mixture. After that, 50 mg of the as-prepared CFG was added into the above clear solution with the help of ultrasound for two hours, and then the suspension was transferred into a 25 mL beaker, which was placed into a 100 mL stainless steel autoclave with a Teflon-liner filled with de-ionized water. The autoclave was heated to 180 °C and kept for 36 h. During the reaction, the de-ionized water vaporized and led to TBOT hydrolysis. At the end of the reaction, the autoclave was cooled to ambient temperature, and the precipitate obtained was repeatedly washed with de-ionized water and ethanol, and then dried at 60 °C in a vacuum oven for 8 h. Furthermore, undoped $CoFe_2O_4@$rGO@TiO_2 (CFGT) was synthesized as above without thiourea.

2.3 Characterization

X-ray powder diffraction (XRD) was used to characterize the phase structures and particle sizes of the as-prepared samples, using a Rigaku D/max 2500 pc X-ray diffractometer with Cu Kα radiation ($\lambda = 1.54056$ Å) at a scan rate of $0.02°$ s^{-1}. The morphology and structure of the catalysts were examined by field emission transmission electron microscopy (HRTEM, JEM-2100F, Japan). Fourier transform infrared (FT-IR) spectra on KBr pellets of the samples were recorded on a PE-100 FT-IR spectrometer at a resolution of 4 cm^{-1}. Diffuse reflectance spectra (DRS) of samples were obtained using a Varian Cary 5000 spectrometer equipped with a Cary Labsphere DRA-CA-301 DR accessory. Photocurrent density was measured by a CHI electrochemical analyzer (CHI 660e, China) in a standard three-electrode configuration, with the working electrode (an effective area of 2 cm^2), a platinum foil as the counter electrode, and a saturated calomel electrode (SCE) as the reference electrode. Na_2SO_4 (0.01 M) was used as the electrolyte. X-ray photoelectron spectroscopy (XPS) was conducted with an ESCALAB250 (Vacuum Generators) spectrometer using monochromatized Al K X-rays (150 W). The magnetic properties of the samples were determined by a vibrating sample magnetometer (VSM, Lake Shore 7410, USA) at a temperature of 300 K.

2.4 Photocatalytic experiments

The photocatalytic performance of the as-prepared samples was evaluated by measuring the decomposition of a 5 mg L^{-1} organic dyes aqueous solution. UV-light photocatalytic experiments were carried out in a homemade jacketed reactor with a 25 W low-pressure mercury lamp as the UV-light source, and the light intensity was 80 μW cm^{-2}. 0.18 g of the as-prepared sample was dispersed in 900 mL of the aqueous dye solution. The Vis-light photocatalytic experiments were carried out in a 250 mL jacketed reactor under a 300 W Xe lamp with a filter to remove light of wavelengths below 420 nm as the Vis-light source, and the light intensity is 240 mW cm^{-2}. 0.08 g of the as-prepared sample was dispersed in 100 mL of the aqueous dye solution. Prior to photocatalytic experiments, the catalysts were settled in suspension for 30 min in the dark for the adsorption equilibrium. The concentration of the organic dye solution was quantified by a Shimadzu UV-2550 (Japan) spectrophotometer at the maximum absorption wavelength of different dyes (λ_{max} (MO) = 464 nm, λ_{max} (MB) = 663 nm and λ_{max} (RhB) = 554 nm). To evaluate the photocatalyst stability, CFGT-S/N were magnetically separated, washed, dried, and reused for the next cycle under the same conditions. The used CFGT-S/N after five cycles was named CFGT-S/N-5. The quenching tests of the active species for the photoreaction were carried out by using different scavengers. The photocatalytic reaction rate constants (k) used the pseudo-first-order model as expressed as eqn (1)

$$\ln(C/C_0) = -kt \tag{1}$$

where C and C_0 were the actual and initial concentrations of the MO solution, respectively, and k was the apparent reaction rate

constant. To ensure the accuracy of the experiment, each experiment was carried out three times.

3 Results and discussion

3.1 XRD analysis and FT-IR measurements

The XRD patterns of CFG, CFGT, CFGT-S/N and CFGT-S/N-5 are shown in Fig. 1(a). It can be easily found that the diffraction peaks of CFG at $2\theta = 30.0°$, $35.4°$, $43.5°$, $57.2°$ and $62.7°$ matched the reflections of (220), (311), (400), (511) and (440), respectively, corresponding to the cubic spinel structure of $CoFe_2O_4$ (JCPDS #79-1744).[31] No apparent diffraction peaks of GO were observed. This was because the crystal growth of $CoFe_2O_4$ between the interlayer of GO destroyed the regular layer stacking, leading to the exfoliation of GO and the disappearance of the (001) diffraction peak during the hydrothermal reaction.[32] After coating with a TiO_2 layer, a new crystalline phase of anatase TiO_2 (JCPDS #21-1272) occurred in the CFGT. However, the diffraction peaks of $CoFe_2O_4$ were weakened, which suggested that most of the $CoFe_2O_4$ NPs were coated with a TiO_2 layer. For the co-doped TiO_2 NPs (CFGT-S/N), the main diffraction peak at $2\theta = 35.4°$ of $CoFe_2O_4$ almost disappeared, suggesting that its saturation magnetization may be decreased. The unit cell volumes of CFGT and CFGT-S/N determined by the Debye–Scherrer equation were 0.1317 and 0.1359 nm^3, which indicated that S and N had been successfully co-doped into the TiO_2 lattice.[8,33] It was noted that the diffraction pattern of CFGT-S/N-5 was almost same as that of CFGT-S/N, which showed that the catalyst possessed a good stability.

In addition, the chemical bonding of the sulfur and nitrogen complexes on the surface of TiO_2 was examined by FT-IR measurements. Fig. 1(b) presented the FT-IR spectra of the samples ranging from 4000 to 400 cm^{-1}. For the CFG NPs, the band was observed in the range 600–500 cm^{-1}, and was indexed to the intrinsic stretching vibrations of the metal at the octahedral site Co–O and Fe–O in $CoFe_2O_4$. The absorption bands at 1230 cm^{-1} and 1076 cm^{-1} were associated with the epoxy C–O and alkoxy C–O groups of GO, respectively.[16,32] The peak at

1627 cm^{-1} corresponded to the O–H bending of the adsorbed water molecules, whereas the broad absorption bands at 3400 cm^{-1} resulted from the O–H stretch region. It can be clearly seen that the main characteristic peaks of the CFG NPs appeared in the spectra of the CFGT NPs and CFGT-S/N NPs, but the GO characteristic peaks were weakened. The absorption bands below 1000 cm^{-1} can be assigned to the Ti–O–Ti vibration.[4] Ammonium ions produced by the dissociation of thiourea were also found in the titania prepared using thiourea as shown by a peak at 1403 cm^{-1} attributable to the deformation mode of ammonium ions.[12] The peak at 1124 cm^{-1} was assigned to the Ti–S vibration, and the peak at 1058 cm^{-1} was ascribed to the Ti–O–S vibration.[13] The above results confirmed that S and N were successfully implanted in the structure of TiO_2.

3.2 UV-Vis DRS spectra analysis

To further investigate the optical properties of the prepared catalysts, the UV-Vis DRS spectra were recorded (Fig. 2). As shown in Fig. 2(a), P25 mainly responded to the ultraviolet region. However, the absorption of TiO_2-SN (T-SN) in the visible light region was significantly increased due to co-doping with N and S elements.[14,42,46] $CoFe_2O_4$ (CF) had broad and obvious absorption ranging in a wide region from 300 to 800 nm owing to its narrow bandgap.[21,23–25,34] CFG NPs showed a stronger light absorption than CF, implying that the introduction of rGO can enhance the visible light absorption.[17,25,36] Compared with CFG, the absorption intensity of CFGT decreased slightly, which can be attributed to the mixing effect of the two semiconductors introducing defect levels.[35] Furthermore, it was found that CFT showed a relatively lower absorption in the visible light region (550–800 nm) than CFGT. After co-doping, the absorption of CFGT-S/N in the visible region improved, hence enhancing the photocatalytic activity.[12,37] The plots of the transformed Kubelka–Munck function *versus* the energy of light were shown in Fig. 2(b). The band gap values of P25, T-SN, CF, CFG, CFT, CFGT and CFGT-S/N were 3.29, 3.08, 1.55, 1.45, 2.33, 2.21 and 2.15 eV, respectively. The results indicated that S, N co-doping,
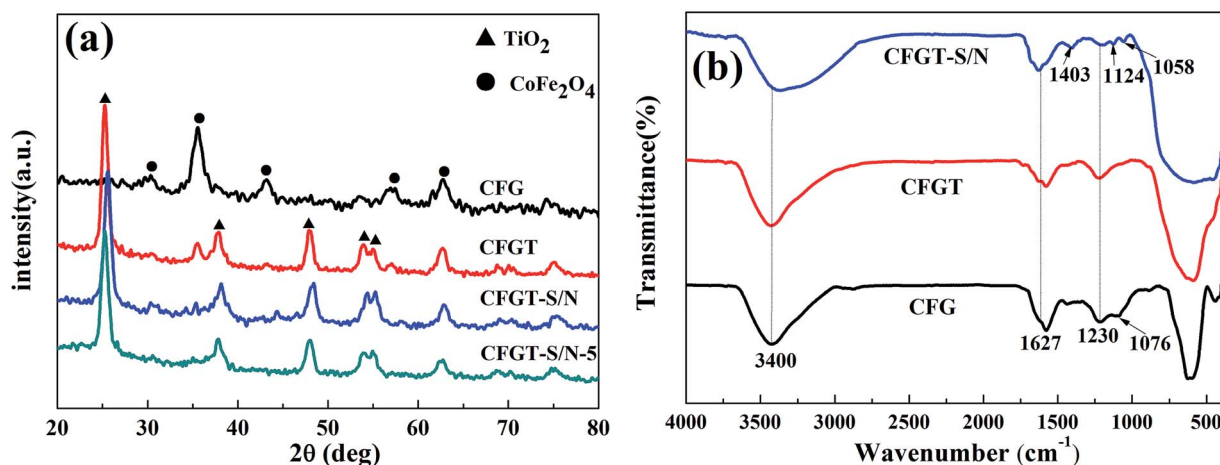

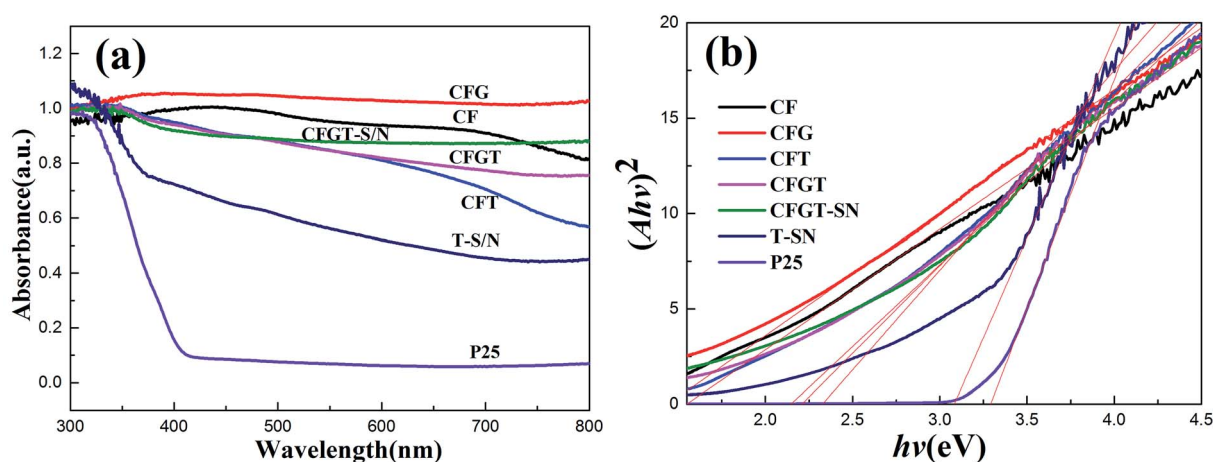Fig. 1   (a) XRD patterns of CFG, CFGT, CFGT-S/N and CFGT-S/N-5; (b) FT-IR spectra of CFG, CFGT, CFGT-S/N.

Fig. 2 (a) Diffuse reflectance spectra (DRS); (b) plots of transferred Kubelka–Munk *vs.* the energy of the light absorbed by the samples.

$CoFe_2O_4$ and rGO can enhance the visible light absorption of CFGT-S/N.

3.3   Morphology and structure analysis

The morphological structure of CFGT-S/N was further verified by FETEM observation. As can be seen in the inset of Fig. 3(a), binary CFG nanoparticles with a core–shell structure can be observed. After TiO_2-S/N coating, CFGT-S/N nanocomposites had a spherical morphology and their grain sizes were 160–220 nm in diameter. From the HRTEM image of the CFGT-S/N hybrid (Fig. 3(b)), two different lattices were observed with *d* spaces of 2.54 and 3.50 Å, corresponding to the (311) plane of $CoFe_2O_4$ and the (101) plane of anatase TiO_2, respectively, which were quite similar to the literature values.[38] In addition, the EDS mapping images clearly showed that Ti, O, C, Fe, Co, S, and N elements were uniformly distributed in the CFGT-S/N sample, further confirming the presence of $CoFe_2O_4$, TiO_2, rGO, and the elements S and N (Fig. 3(d–j)).

3.4   XPS analysis

In order to determine the surface chemical compositions, XPS analysis was carried out. As shown in Fig. 4(a), CFGT contained Fe, Co, C, Ti and O, while CFGT-S/N not only contained Fe, Co, C, Ti, and O, but also S and N, which indicated that S and N had been co-doped into the CFGT-S/N hybrids. As shown in Fig. 4(b), the XPS spectrum of Fe 2p depicted two main broad peaks, 710.9 eV for Fe $2p_{3/2}$ and 724.0 eV for Fe $2p_{1/2}$, and a small peak at 714.3 eV for Fe $2p_{3/2}$, which could be due to the contributions from Fe^{3+} ions. From Fig. 4(c), the peaks of 779.0 eV, 781.0 eV and 794.2 eV were associated with Co^{2+} ions.[21,39] The C 1s high-resolution spectrum was curve-fitted in Fig. 4(d). The peaks at 284.7, 285.8, 286.9 and 288.6 eV were assigned to C=C/C–C, C–OH, C–O and HO–C=O, respectively.[25] For the S 2p XPS spectrum in Fig. 4(e), the characteristic peak in the range of 160–163 eV could be ascribed to the formation of Ti–S bond. It can be deduced that the S^{2-} ions replaced the O^{2-} ions in the lattice of TiO_2, making it produce a lattice distortion due to a large ionic radius difference between S^{2-} (0.184 nm) and O^{2-} (0.140 nm).[12,33]

The peak at 168.8 eV was related to the S^{6+} of SO_4^{2-} ions, assigned to the SO_4^{2-} ions adsorbed on the surface of CFGT-S/N.[41] The XPS spectra of the N 1s region are shown in Fig. 4(f). The peak at 400.3 eV was attributed to interstitial nitrogen atoms as Ti–O–N structural characteristic.[10,13] From Fig. 4(g), the Ti 2p XPS spectrum of CFGT-S/N appeared two peaks at 459.2 and 465.0 eV, assigned to Ti $2p_{3/2}$ and Ti $2p_{1/2}$, respectively,[22,40] a little lower than those of CFGT (459.5 and 465.1 eV), which could be attributed to partial of oxygen in the lattice of TiO_2 replaced by low electronegativity S anions, subsequently leading to the increase of the charge density of Ti atoms, and then decreasing binding energy of Ti 2p.[42] This consequence further approved the formation of Ti–S bond. In addition, there is a shift of the O 1s peak by 0.1 eV toward low energy in CFGT-S/N (Fig. 4(h)), indicating the existence of concomitant oxygen deficiencies, which resulted in increased outer electron density of O and, consequently, decreased binding energy.[43,50] The result of XPS was in good agreement with FT-IR.

3.5   Magnetic characterization

To evaluate the magnetic separation capacity, the magnetic hysteresis loops of CFG, CFGT and CFGT-S/N nanoparticles were measured at room temperature, as shown in Fig. 5. The saturation magnetization (Ms) values of the CFG, CFGT and CFGT-S/N were 32.74, 2.95 and 1.73 emu g^{-1}, respectively. It can be found that the non-magnetic coating TiO_2 layer affected the magnetic properties of the $CoFe_2O_4$ particles.[20,23] Fortunately, the maximum saturation magnetization of 1.73 emu g^{-1} was strong enough to separate CFGT-S/N from solution with the help of an external magnetic force. The magnetic separability was tested by placing a magnet near a glass bottle. The black product was rapidly attracted toward the magnet in a short period (the inset of Fig. 5), demonstrating the high magnetic sensitivity of the CFGT-S/N nanocomposites.

3.6   Photocatalytic activities

3.6.1   Photodegradation of MO. The photocatalytic activities of CFT, CFGT, CFGT-S/N, P25, and $CoFe_2O_4$ were tested
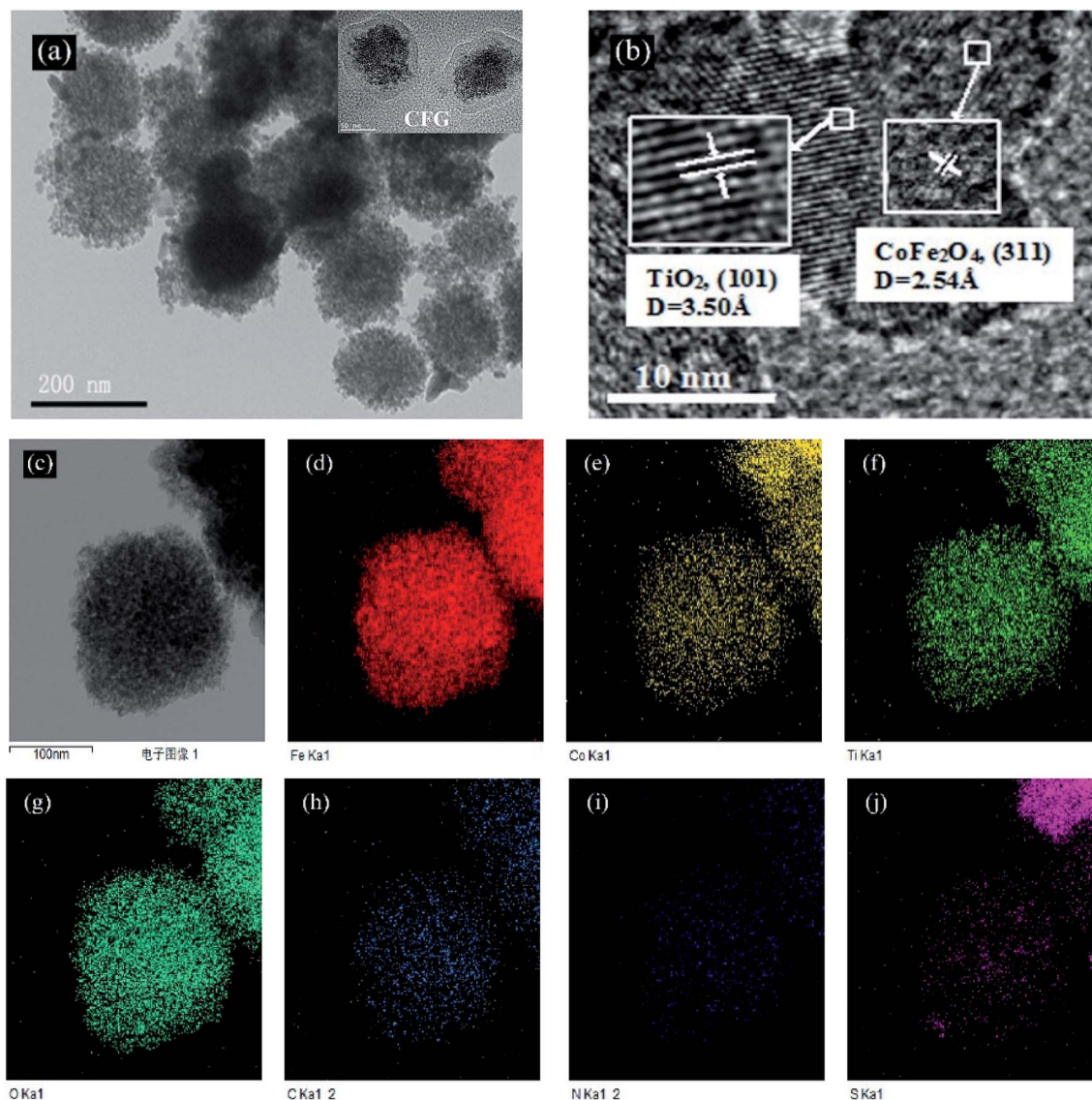
Fig. 3 (a) and (c) FETEM and (b) HRTEM images of CFGT-S/N; EDS elemental mapping images of the corresponding area: (d) Fe; (e) Co; (f) Ti; (g) O; (h) C; (i) N; and (j) S.

using the degradation of MO under UV- and Vis-light irradiation and the results were displayed in Fig. 6. From Fig. 6(a), it can be seen that CF displayed poor UV-light photocatalytic activity and P25 exhibited the highest photocatalytic activity. For CFT, MO degradation rate was only 74% within 150 min, while for CFGT, 100% of MO was degraded due to the rGO acting as an acceptor of the electrons generated in the TiO$_2$ particles, suppressing the recombination of charges.[26] After S, N co-doping, CFGT-S/N exhibited an improved photocatalytic activity compared to CFGT, and it took around 120 min to decompose MO completely. Furthermore, Fig. 6(b) illustrates that the photocatalytic reaction rate constants (k) onto CF, CFT, CFGT, CFGT-S/N and P25, were in turn 0.0009, 0.0081, 0.0133, 0.0192 and 0.1014 min^{-1}. Due to the lower content of TiO$_2$ in CFGT-S/N at the same dosage of catalysts, its rate constant k was lower than that of P25. As shown in Fig. 6(c), almost no degradation of MO over bare CF and CFT was observed under visible light

irradiation. Although CFGT exerted facile MO adsorption, it displayed less photocatalytic activity. Notably, CFGT-S/N exhibited better catalytic activity, and the degradation rate of MO reached 100% within 6 h. For P25, only 72% of MO was removed within 6 h. It can be seen from Fig. 6(d), the k of CF, CFT, CFGT, CFGT-S/N and P25 was 0, 0, 0.0003, 0.0052 and 0.0039 min^{-1}, respectively. The k of CFGT-S/N was 33% higher than that of P25 under visible light irradiation. It indicated that the prepared CFGT-S/N displayed an excellent photocatalytic activity no matter which light source (UV or Vis) was used.

3.6.2 Photodegradation of various dyes. The photodegradation of the different organic dyes on CFGT-S/N was further studied under UV- and Vis-light irradiation. Two kinds of anionic dyes (RhB and MB) were selected as other pollutants. To confirm whether dyes were not photodegraded by itself, a blank test was also carried out. As shown in Fig. 7(a), CFGT-S/N exhibited excellent UV-light photocatalytic activity, and it only
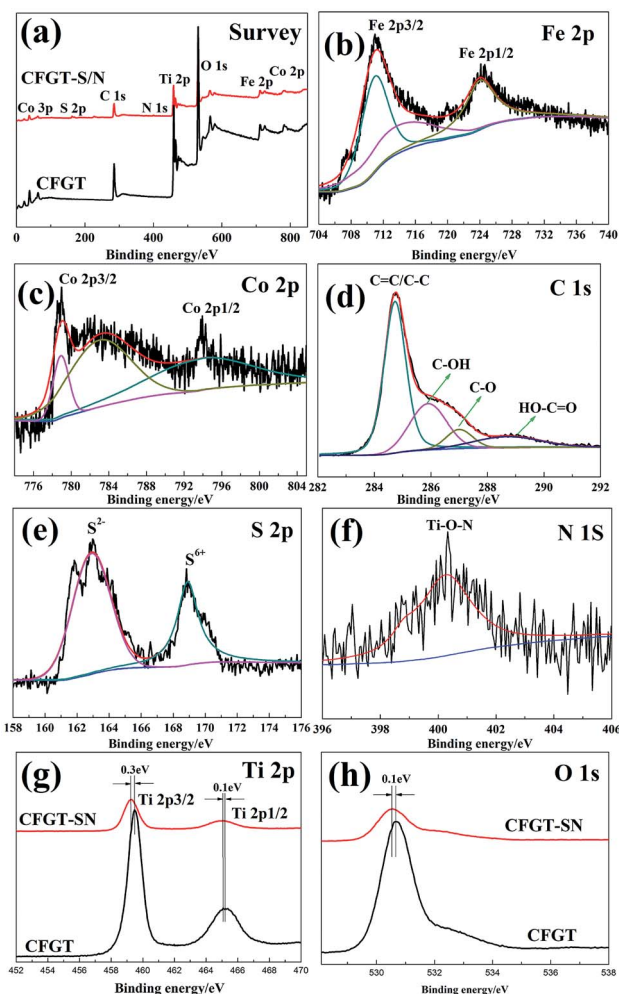
Fig. 4 (a) XPS survey spectra of CFGT and CFGT–S/N; high-resolution spectra of (b) Fe 2p, (c) Co 2p, (d) C 1s, (e) S 2p and (f) N 1s of CFGT–S/N; and high-resolution spectra of (g) Ti 2p and (h) O 1s of CFGT and CFGT–S/N.
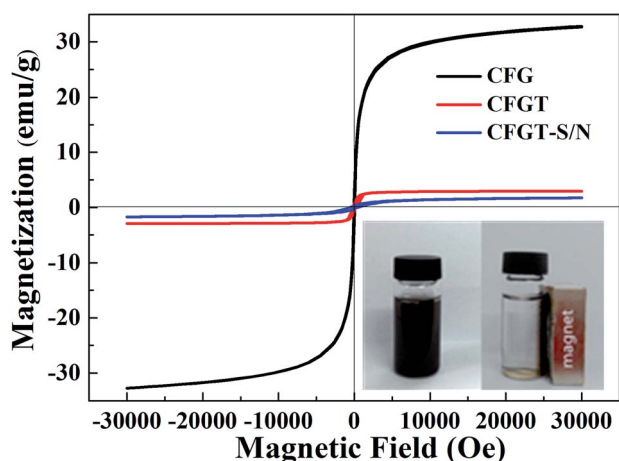

Fig. 5 VSM magnetization curves of CFG, CFGT and CFGT–S/N. The inset shows the separation of CFGT–S/N from aqueous solution under an external magnetic field.

took 120 min to decompose various pollutants molecules completely. Under Vis-light illumination, the photocatalytic degradation rates of pollutants were still lower than those under UV-light illumination as shown in Fig. 7(b). Overall, the CFGT–S/N showed no selectivity to photocatalytic degradation for most organic pollutants, which was of great importance to practical applications.

3.6.3 Cycling photodegradation of MO. As a recyclable photocatalyst, high stability and facile separation of catalysts were also important for the photocatalytic nanomaterial in water remediation.[4] Recycling photocatalytic experiments of CFGT–S/N were conducted, and the results are represented in Fig. 8(a and b). After five cycles, the degradation rates of MO were 96% and 92% of that for the first cycle under UV- and Vis-light illumination, respectively. This result implied that the as-prepared catalysts had an excellent chemical stability and could be recycled in the organic dyestuff wastewater purification.

3.7 Photocatalytic mechanism

To better understand the separation efficiency of the photo-generated electrons and holes of CFGT–S/N, we investigated its photoinduced charge transfer properties.[5] Fig. 9(a) shows the photocurrent density variations of the P25, CFG, CFT, CFGT and CFGT–S/N electrodes with measured potential in Na_2SO_4 solution. The dark current densities in all cases can be negligible. Upon irradiation, a significant increase in the photocurrent density was observed throughout the potential window at the CFGT–S/N electrode. The saturated photocurrent density of the CFGT–S/N electrode was about 0.71 $\mu A\ cm^{-2}$, higher than those of the CFGT (0.08 $\mu A\ cm^{-2}$), CFT (0.05 $\mu A\ cm^{-2}$), CFG (0.05 $\mu A\ cm^{-2}$) and P25 (0.06 $\mu A\ cm^{-2}$) electrodes by a factor of 11.8, 14.2, 14.2 and 8.9, respectively. This demonstrated that the separation rate of photo-generated electrons and holes increased because of the co-doping of S and N in the TiO_2 network.

Furthermore, to verify the role of the reactive species under UV-Vis light irradiation over CFGT–S/N, different scavengers were employed in this study. They were benzoquinone (0.1 mM BQ) for the superoxide radical ($O_2{}^{\bullet-}$), *tert*-butyl alcohol (0.1 mM TBA) for the hydroxyl radical ($\cdot OH$), $AgNO_3$ (0.01 mM) for photogenerated electrons (e^-) and disodium ethylenediamine-tetraacetate (0.1 mM EDTA) for photo-generated holes (h^+).[3,4] As shown in Fig. 9(b), upon the addition of BQ and EDTA, the degradation rates were greatly suppressed to 23% and 48%, respectively. After the addition of $AgNO_3$, the photodegradation rate of MO decreased from 100% to 68%, indicating that e^- was definitely produced and transferred from TiO_2-SN to rGO in the photocatalytic reaction, which was consistent with the literature reports.[47,50] Besides, a significant change was observed in the presence of TBA, displaying that $\cdot OH$ as an oxidation species was also indeed photogenerated on catalyst surfaces. The results suggested that $O_2{}^{\bullet-}$, h^+, e^- and $\cdot OH$ were the main active species in the MO photocatalytic oxidation process.

On the basis of the above experimental results, a possible photocatalytic mechanism for CFGT–S/N under UV-Vis irradiation was proposed and is illustrated in Scheme 1. Upon UV-Vis irradiation, $CoFe_2O_4$ (1.55 eV) with a narrow bandgap energy
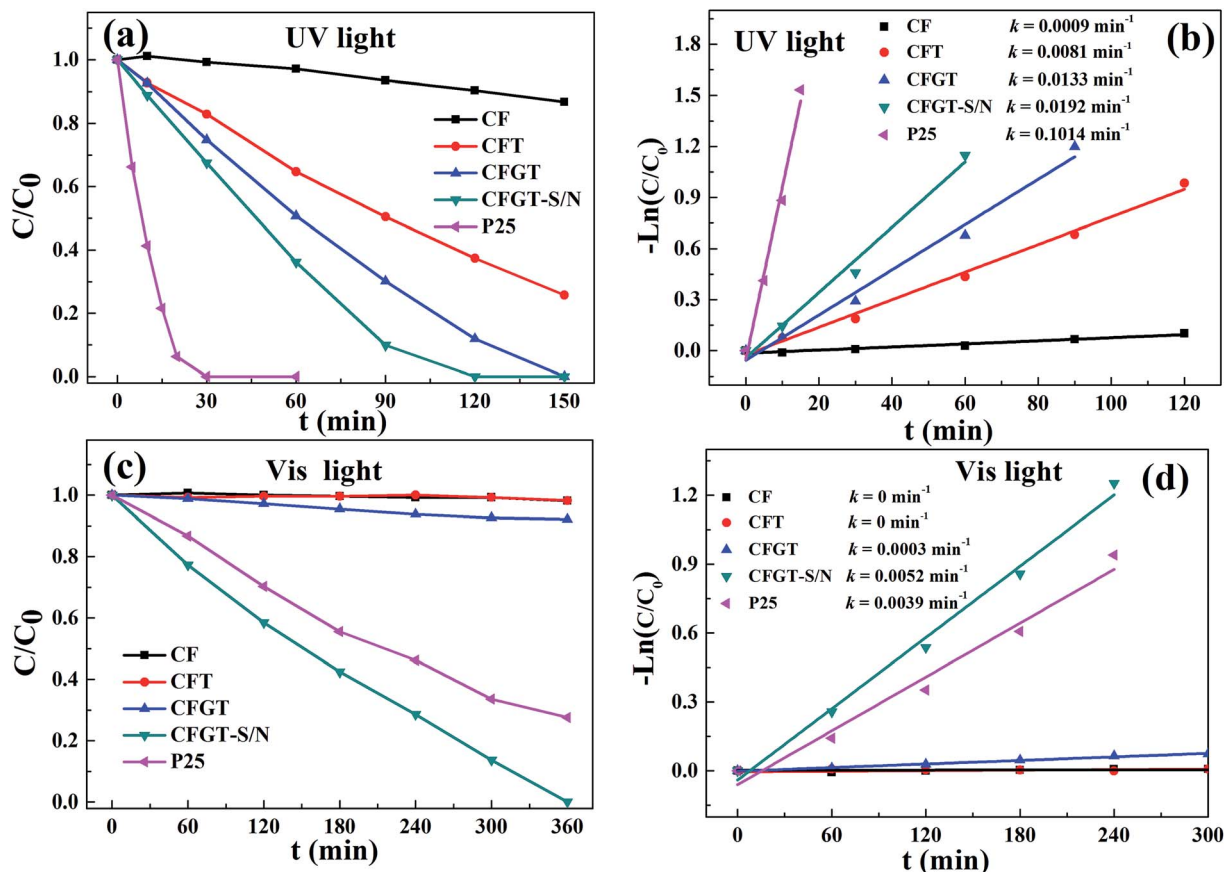
Fig. 6 Photodegradation of MO on CF, P25, CFT, CFGT and CFGT-S/N under (a) UV- and (c) Vis-light irradiation; (b) and (d) first-order kinetics rate curves.

could be easily excited from the valence band (VB) to the conduction band (CB), inducing the generation of electron–hole pairs (eqn (2)).[24,25,44,45] Notably, the introduction of CoFe$_2$O$_4$ with superparamagnetic behavior was conducive to catalyst recycling.[23,25] For TiO$_2$, the co-doping of nitrogen and sulfur into the TiO$_2$ lattice led to the formation of mid-gap energy levels such as N 2p and S 2p between the valence band (VB) of O 2p and the conduction band (CB) of Ti 3d and narrowed the bandgap energy to 3.08 eV, thereby TiO$_2$-S/N can be excited easily by the

photons (eqn (3)).[42,46,52,53] The photoinduced electrons (e$^-$) from TiO$_2$-S/N can be quickly transferred to the huge π–π network of rGO due to their excellent electron accepting and transporting properties,[36,47] and then rGO (e$^-$) reacted with dissolved O$_2$ to generate O$_2$$^{\cdot-}$ radicals (eqn (4) and (5)). This process can restrain effectively the electron–hole recombination on TiO$_2$-S/N.[48,49] The photoinduced holes (h$^+$) remaining in the VB of TiO$_2$-SN can directly degrade MO, and can also be captured by H$_2$O to form ·OH radicals (eqn (6)).[45,46,50] Moreover, the h$^+$ on the VB of
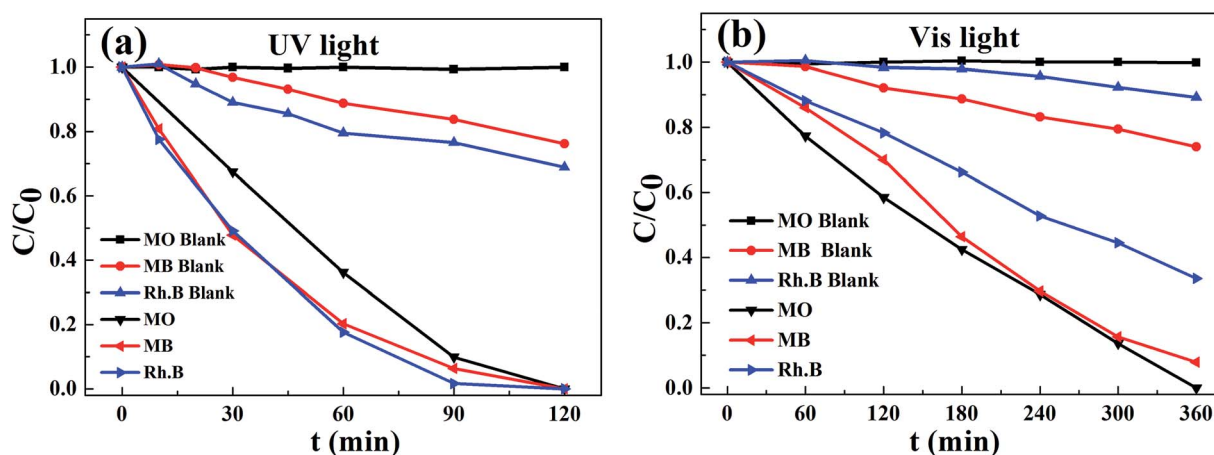

Fig. 7 Photodegradation of various dyes in the presence of CFGT-S/N under (a) UV- and (b) Vis-light irradiation.
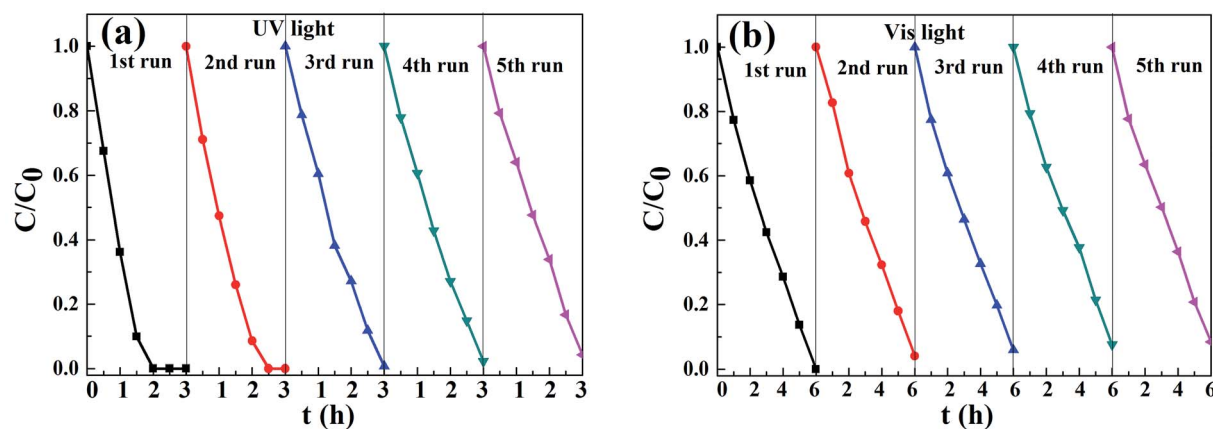
Fig. 8 Cycling photodegradation of MO on CFGT-S/N under (a) UV- and (b) Vis-light irradiation.
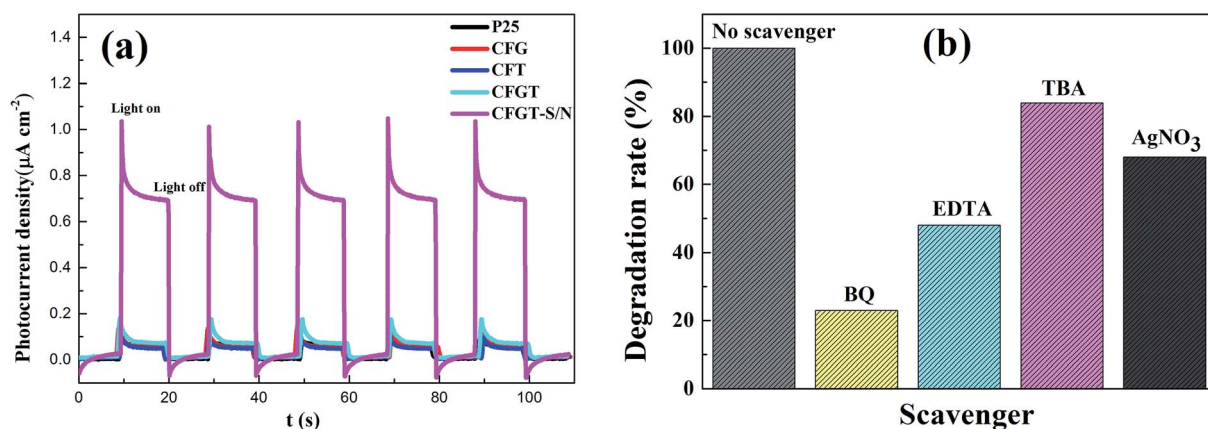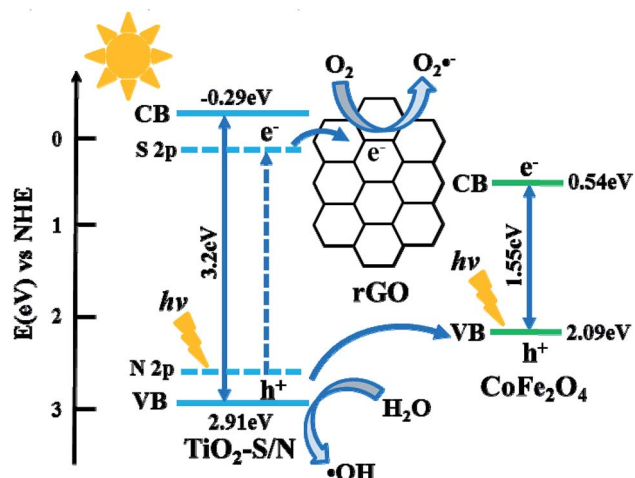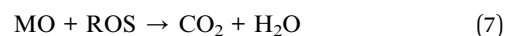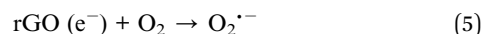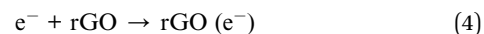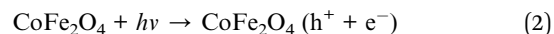

Fig. 9 (a) Photocurrent density of P25, CFG, CFT, CFGT and CFGT-S/N; and (b) photocatalytic activities of CFGT-S/N hybrid in the presence of different scavengers under UV-Vis light irradiation (reaction conditions: [MO] = 5 mg L^{-1}, [catalyst] = 0.20 g L^{-1}).

Scheme 1 The possible photocatalytic mechanism on the CFGT-S/N nanocomposite.

TiO_2-S/N can be transferred to the VB of $CoFe_2O_4$ due to the lower potential energy of the VB of $CoFe_2O_4$, which can facilitate efficiently interface charge separation and hamper carrier

recombination.[44,51] As a result, these highly reactive oxygen species (ROS, such as $O_2{}^{\bullet-}$, h$^+$ and $\cdot$OH) can effectively degrade MO adsorbed on CFGT-SN (eqn (7)). According to the above analysis, the relevant reactions on the surface of nanocomposite can be expressed as follows:

$$CoFe_2O_4 + h\nu \rightarrow CoFe_2O_4\ (h^+ + e^-) \tag{2}$$

$$TiO_2\text{-S/N} + h\nu \rightarrow TiO_2\text{-S/N}\ (h^+ + e^-) \tag{3}$$

$$e^- + rGO \rightarrow rGO\ (e^-) \tag{4}$$

$$rGO\ (e^-) + O_2 \rightarrow O_2{}^{\bullet-} \tag{5}$$

$$h^+ + H_2O \rightarrow H^+ + \cdot OH \tag{6}$$

$$MO + ROS \rightarrow CO_2 + H_2O \tag{7}$$

4 Conclusions

In summary, we have presented a simple and controllable way to synthesise magnetically separable S, N co-doped

$CoFe_2O_4@rGO@TiO_2$ composites, which has not been reported before. This method can efficiently dope sulfur and nitrogen elements into the lattice of TiO_2. The results showed that CFGT-S/N exhibited excellent photocatalytic activity no matter which light source (UV or Vis) was used. The high activity of CFGT-S/N was ascribed to a synergetic consequence of several beneficial effects, such as the efficient separation of photoinduced electron–hole pairs and the improvement in UV-Vis absorption. Furthermore, the presence of $CoFe_2O_4$ in the hybrid helped the catalyst particles to acquire ferromagnetic properties, and they were easily separated from the catalytic solution. Therefore, the synthesized CFGT-S/N can be used as a composite photocatalyst for the elimination of organic pollutants from waste water.

Conflicts of interest

There are no conflicts to declare.

Acknowledgements

References

1 J. Schneider, M. Matsuoka, M. Takeuchi, J. L. Zhang, Y. Horiuchi, M. Anpo and D. W. Bahnemann, Understanding TiO_2 photocatalysis: mechanisms and materials, *Chem. Rev.*, 2014, **114**(19), 9919–9986.

2 M. Liu, R. Inde, M. Nishikawa, X. Q. Qiu, D. Atarashi, E. Sakai, Y. Nosaka, K. Hashimoto and M. Miyauchi, Enhanced photoactivity with nanocluster-grafted titanium dioxide photocatalysts, *ACS Nano*, 2014, **8**(7), 7229–7238.

3 C. Burda and X. Chen, The electronic origin of the visible-light absorption properties of C-, N- and S-doped TiO_2 nanomaterials, *J. Am. Chem. Soc.*, 2008, **130**(15), 5018–5019.

4 Y. J. Yao, J. C. Qin, H. Chen, F. Y. Wei, X. T. Liu, J. L. Wang and S. B. Wang, One-pot approach for synthesis of N-doped $TiO_2/ZnFe_2O_4$ hybrid as an efficient photocatalyst for degradation of aqueous organic pollutants, *J. Hazard. Mater.*, 2015, **291**, 28–37.

5 F. Y. Wei, T. Liu, F. Z. Zhou, W. Ran, Y. J. Yao, H. Wang and P. H. Wang, Magnetic recoverable F-N Co-doped $ZnFe_2O_4/C/TiO_2$ nanocomposites with UV-Vis light photocatalytic activity, *Environ. Eng. Sci.*, 2018, **35**, 37–45.

6 T. Ohno, M. Akiyoshi, T. Umebayashi, K. Asai, T. Mitsui and M. Matsumura, Preparation of S-doped TiO_2 photocatalysts and their photocatalytic activities under visible light, *Appl. Catal., A*, 2004, **265**(1), 115–121.

7 Y. M. Wu, M. Y. Xing, J. L. Zhang and F. Chen, Effective visible light-active boron and carbon modified TiO_2 photocatalyst for degradation of organic pollutant, *Appl. Catal., B*, 2010, **97**, 182–189.

8 M. Behpour, R. Foulady-Dehaghi and N. Mir, Considering photocatalytic activity of N/F/S-doped TiO_2 thin films in degradation of textile waste under visible and sunlight irradiation, *Sol. Energy*, 2017, **158**, 636–643.

9 S. In, A. Orlov, R. Berg, F. García, S. Pedrosa-Jimenez, M. S. Tikhov, D. S. Wright and R. M. Lambert, Effective visible light-activated B-doped and B,N-codoped TiO_2 photocatalysts, *J. Am. Chem. Soc.*, 2007, **129**(45), 13790–13791.

10 X. P. Wang and T. Lim, Solvothermal synthesis of C-N codoped TiO_2 and photocatalytic evaluation for bisphenol a degradation using a visible-light irradiated LED photoreactor, *Appl. Catal., B*, 2010, **100**, 355–364.

11 N. C. Birben, C. S. Uyguner-Demirel, S. Sen-Kavurmaci, Y. Y. Gurkan, N. Turkten, Z. Cinar and M. Bekbolet, Comparative evaluation of anion doped photocatalysts on the mineralization and decolorization of natural organic matter, *Catal. Today*, 2015, **240**, 125–131.

12 F. Y. Wei, L. S. Ni and P. Cui, Preparation and characterization of N-S-codoped TiO_2 photocatalyst and its photocatalytic activity, *J. Hazard. Mater.*, 2008, **156**, 135–140.

13 G. Zhang, C. Z. Yong, M. Nadagouda, C. Han, K. O'Shea, S. M. El-Sheikh, A. A. Ismail and D. D. Dionysiou, Visible light-sensitized S, N and C co-doped polymorphic TiO_2 for photocatalytic destruction of microcystin-LR, *Appl. Catal., B*, 2014, **144**(1), 614–621.

14 W. W. Zhao, F. H. Tian, X. B. Wang, L. H. Zhao, L. H. Xia and C. B. Liu, Theoretical study on S-, N-doped anatase TiO_2: the visible-light-driven photocatalysts, *Journal of Computational Science & Engineering*, 2013, **4**, 170–177.

15 Q. Y. He, H. G. Sudibya, Z. Y. Yin, S. X. Wu, H. Li, F. Boey, W. Huang, P. Chen and H. Huang, Centimeter-long and large-scale micropatterns of reduced graphene oxide films: fabrication and sensing applications, *ACS Nano*, 2010, **4**, 3201–3208.

16 D. Y. Liang, C. Cui, H. H. Hu, Y. P. Wang, S. Xu, B. L. Ying, P. G. Li, B. Q. Lu and H. L. Shen, One-step hydrothermal synthesis of anatase TiO_2/reduced graphene oxide nanocomposites with enhanced photocatalytic activity, *J. Alloys Compd.*, 2014, **582**, 236–240.

17 Z. Q. Li, H. L. Wang, L. Y. Zi, J. J. Zhang and Y. S. Zhang, Preparation and photocatalytic performance of magnetic $TiO_2–Fe_3O_4$/graphene (RGO) composites under Vis-light irradiation, *Ceram. Int.*, 2015, **41**, 10634–10643.

18 H. Liu, X. N. Dong, X. C. Wang, C. C. Sun, J. Q. Li and Z. F. Zhu, A green and direct synthesis of graphene oxide encapsulated TiO_2 core/shell structures with enhanced photoactivity, *Chem. Eng. J.*, 2013, **230**, 279–285.

19 H. Kim, G. Moon and M. Damian, Solar photoconversion using Graphene/TiO_2 composites: nanographene shell on TiO_2 core *versus* TiO_2 nanoparticles on graphene sheet, *J. Phys. Chem. C*, 2012, **116**, 1535–1543.

20 P. C. Ma, W. Jiang, F. H. Wang, F. S. Li, P. Shen, M. D. Chen, Y. J. Wang, J. Liu and P. Y. Li, Synthesis and photocatalytic property of $Fe_3O_4@TiO_2$ core/shell nanoparticles supported by reduced graphene oxide sheets, *J. Alloys Compd.*, 2013, **578**, 501–506.

21 V. K. Gupta, T. Eren, N. Atar, M. L. Yole, C. Parlak and H. Karimi-Maleh, $CoFe_2O_4@TiO_2$ decorated reduced graphene oxide nanocomposite for photocatalytic degradation of chlorpyrifos, *J. Mol. Liq.*, 2015, **208**, 122–129.

22 J. T. Feng, Y. C. Wang, Y. H. Hou and L. C. Li, Tunable design of yolk–shell ZnFe$_2$O$_4$@RGO@TiO$_2$ microspheres for enhanced high-frequency microwave absorption, *Inorg. Chem. Front.*, 2017, **4**, 935–945.

23 S. M. Moosavi, P. Molla-Abbasi and Z. Haji-Aghajani, Photocatalyst CoFe$_2$O$_4$–TiO: application in photo-degradation of organic dyes and magnetic nanocomposite preparation, *J. Mater. Sci.: Mater. Electron.*, 2016, **27**, 4879–4886.

24 P. Sathishkumar, R. V. Mangalaraja, S. Anandan and M. Ashokkumar, CoFe$_2$O$_4$/TiO$_2$, nanocatalysts for the photocatalytic degradation of reactive red 120 in aqueous solutions in the presence and absence of electron acceptors, *Chem. Eng. J.*, 2013, **220**, 302–310.

25 J. W. Sun, Y. S. Fu, P. Xiong, X. Q. Sun, B. H. Xu and X. Wang, A magnetically separable P25/CoFe$_2$O$_4$/graphene catalyst with enhanced adsorption capacity and visible-light-driven photocatalytic activity, *RSC Adv.*, 2013, **3**, 22490–22497.

26 Y. Lin, Z. G. Geng, H. B. Cai, L. Ma, J. Chen, J. Zeng, N. Pan and X. P. Wang, Ternary graphene–TiO$_2$–Fe$_3$O$_4$ nanocomposite as a recollectable photocatalyst with enhanced durability, *Eur. J. Inorg. Chem.*, 2012, **28**, 4439–4444.

27 S. M. Li, B. Wang, J. H. Liu and M. Yu, In situ one-step synthesis of CoFe$_2$O$_4$/graphene nanocomposites as high performance anode for lithium-ion batteries, *Electrochim. Acta*, 2014, **129**, 33–39.

28 X. L. Yang, W. Chen, J. F. Huang, Y. Zhou, Y. H. Zhu and C. Z. Li, Rapid degradation of methylene blue in a novel heterogeneous Fe$_3$O$_4$@rGO@TiO$_2$-catalyzed photo-fenton system, *Sci. Rep.*, 2015, **5**, 10632–10642.

29 Z. J. Song, W. Ran and F. Y. Wei, One-step approach for the synthesis of CoFe$_2$O$_4$@rGO core-shell nanocomposites as efficient absorbent for removal of organic pollutants, *Water Sci. Technol.*, 2017, **75**, 397–405.

30 D. C. Marcano, D. V. Kosynkin, J. M. Berlin, A. Sinitskii, Z. Z. Sun, A. Slesarev, L. B. Alemany, W. Lu and J. M. Tour, Improved synthesis of graphene oxide, *ACS Nano*, 2010, **4**, 4806–4814.

31 Y. J. Yao, Z. H. Yang, D. W. Zhang, W. H. Peng, H. Q. Sun and S. Wang, Magnetic CoFe$_2$O$_4$-graphene hybrids: facile synthesis, characterization, and catalytic properties, *Ind. Eng. Chem. Res.*, 2012, **51**, 6044–6051.

32 L. Gan, S. M. Shang, C. W. M. Yuen, S. X. Jiang and E. L. Hu, Hydrothermal synthesis of magnetic CoFe$_2$O$_4$/graphene nanocomposites with improved photocatalytic activity, *Appl. Surf. Sci.*, 2015, **351**, 140–147.

33 D. Ma, Y. J. Xin, M. C. Gao and J. Wu, Fabrication and photocatalytic properties of cationic and anionic S-doped TiO$_2$ nanofibers by electrospinning, *Appl. Catal., B*, 2014, **147**, 49–57.

34 M. H. Habibi and J. Parhizkar, Cobalt ferrite nano-composite coated on glass by doctor blade method for photo-catalytic degradation of an azo textile dye reactive red 4: XRD, FESEM and DRS investigations, *Spectrochim. Acta, Part A*, 2015, **150**, 879–885.

35 P. P. Hankare, R. P. Patil, A. V. Jadhav, K. M. Garadkar and R. Sasikala, Enhanced photocatalytic degradation of methyl red and thymol blue using titania–alumina–zinc ferrite nanocomposite, *Appl. Catal., B*, 2011, **107**, 333–339.

36 G. Y. He, J. J. Ding, J. G. Zhang, Q. L. Hao and H. Q. Chen, One-step ball-milling preparation of highly photocatalytic active CoFe$_2$O$_4$-reduced graphene oxide heterojunctions for organic dye removal, *Ind. Eng. Chem. Res.*, 2015, **54**, 2862–2867.

37 M. Behpour and V. Atouf, Study of the photocatalytic activity of nanocrystalline S, N-codoped TiO$_2$ thin films and powders under visible and sun light irradiation, *Appl. Surf. Sci.*, 2012, **258**(17), 6595–6601.

38 W. Li, J. P. Yang, Z. X. Wu, J. X. Wang, B. Li, S. S. Feng, Y. H. Deng, F. Zhang and D. Y. Zhao, A versatile kinetics-controlled coating method to construct uniform porous TiO$_2$ shells for multifunctional core-shell structures, *J. Am. Chem. Soc.*, 2012, **134**, 11864–11867.

39 Z. P. Zhou, Y. Zhang, Z. Y. Wang, W. Wei, W. F. Tang, J. Shi and R. Xiong, Electronic structure studies of the spinel CoFe$_2$O$_4$ by X-ray photoelectron spectroscopy, *Appl. Surf. Sci.*, 2008, **254**, 6972–6975.

40 Y. Min, G. Q. He, R. B. Li, W. Zhao, Y. C. Chen and Y. G. Zhang, Doping nitrogen anion enhanced photocatalytic activity on TiO$_2$ hybridized with graphene composite under solar light, *Sep. Purif. Technol.*, 2013, **106**, 97–104.

41 C. Han, M. Pelaez, V. Likodimos, A. G. Kontos, P. Falaras, K. Shea and D. D. Dionysiou, Innovative visible light-activated sulfur doped TiO$_2$ films for water treatment, *Appl. Catal., B*, 2011, **107**, 77–87.

42 D. Li, Z. P. Xing, X. J. Yu and X. W. Cheng, One-step hydrothermal synthesis of C-N-S-tridoped TiO$_2$-based nanosheets photoelectrode for enhanced photoelectrocatalytic performance and mechanism, *Electrochim. Acta*, 2015, **170**, 182–190.

43 R. Huo, J. Y. Yang, Y. Q. Liu, H. F. Liu, X. Li and Y. H. Xu, Preparation of W and N, S co-doped titanium dioxide with enhanced photocatalytic activity under visible light irradiation, *Mater. Res. Bull.*, 2016, **76**, 72–78.

44 C. Haw, W. Chiu, S. A. Rahman, P. Khiew, S. Radiman, R. A. Shukor, M. A. A. Hamid and N. Ghazali, The design of new magnetic-photocatalyst nanocomposites (CoFe$_2$O$_4$-TiO$_2$) as smart nanomaterials for recyclable-photocatalysis applications, *New J. Chem.*, 2016, **40**, 1124–1136.

45 P. Xiong, L. J. Wang, X. Q. Sun, B. H. Xu and X. Wang, Ternary titania-cobalt ferrite-polyaniline nanocomposite: a magnetically recyclable hybrid for adsorption and photodegradation of dyes under visible light, *Ind. Eng. Chem. Res.*, 2013, **52**, 10105–10113.

46 A. Brindha and T. Sivakumar, Visible active N, S co-doped TiO$_2$/graphene photocatalysts for the degradation of hazardous dyes, *J. Photochem. Photobiol., A*, 2017, **340**, 146–156.

47 Q. W. Huang, S. Q. Tian, D. W. Zeng, X. X. Wang, W. L. Song, Y. Y. Li, W. Xiao and C. S. Xie, Enhanced photocatalytic activity of chemically bonded TiO$_2$/graphene composites based on the effective interfacial charge transfer through the C–Ti bond, *ACS Catal.*, 2013, **3**(7), 1477–1485.

48 P. Wang, J. Wang, T. S. Ming, X. F. Wang, H. G. Yu, J. G. Yu, Y. G. Wang and M. Lei, Dye-sensitization-induced visible-light reduction of graphene oxide for the enhanced TiO_2 photocatalytic performance, *ACS Appl. Mater. Interfaces*, 2013, **5**(8), 2924.

49 H. Zhang, X. J. Lv, Y. M. Li, Y. Wang and J. H. Li, P25-graphene composite as a high performance photocatalyst, *ACS Nano*, 2010, **4**(1), 380–386.

50 W. Qian, P. A. Greaney, S. Fowler, S. K. Chiu, A. M. Gafoth and J. Jiao, Low-temperature titrogen doping in ammonia solution for production of N-doped TiO_2-hybridized graphene as a highly efficient photocatalyst for water treatment, *ACS Sustainable Chem. Eng.*, 2014, **2**(7), 1802–1810.

51 C. J. Leng, J. H. Wei, Z. Y. Liu, R. Xiong, C. X. Pan and J. Shi, Facile synthesis of PANI-modified $CoFe_2O_4$-TiO_2, hierarchical flower-like nanoarchitectures with high photocatalytic activity, *J. Nanopart. Res.*, 2013, **15**(5), 1–11.

52 C. Di Valentin, G. Pacchioni, A. Selloni, S. Livraghi and E. Giamello, Characterization of paramagnetic species in N-doped TiO_2 powders by EPR spectroscopy and DFT calculations, *J. Phys. Chem. B*, 2005, **109**(23), 11414–11419.

53 S. Pany, B. Naik, S. Martha and K. Parida, Plasmon induced nano Au particle decorated over S,N-modified TiO_2 for exceptional photocatalytic hydrogen evolution under visible light, *ACS Appl. Mater. Interfaces*, 2014, **6**(2), 839–846.